Materials Today Bio 28 (2024) 101239

Contents lists available at ScienceDirect

Materials Today Bio

journal homepage: www.journals.elsevier.com/materials-today-bio

Polymeric PD1/PDL1 bispecific antibody enhances immune checkpoint blockade therapy

Fuxin Xue [a], Xitong Ren [b], Chaoying Kong [b], Jianfeng Wang [a], Linlin Liu [a,*], Junli Hu [c,**], Na Shen [b,***], Zhaohui Tang [b]

[a] Department of Radiation Oncology, China-Japan Union Hospital of Jilin University, Changchun, Jilin, 130033, China
[b] Key Laboratory of Polymer Ecomaterials, Changchun Institute of Applied Chemistry, Chinese Academy of Sciences, Changchun, Jilin, 130022, China
[c] Key Laboratory of UV-Emitting Materials and Technology, Northeast Normal University, Ministry of Education, Changchun, Jilin, 130024, China

ARTICLE INFO

Keywords:
T cell engager
Bispecific antibody
PD1/PDL1 blockage
Cancer immunotherapy
Fc binding peptide

ABSTRACT

Immune checkpoint blockade (ICB) therapy, particularly PD1/PDL1 inhibition, has demonstrated success in bolstering durable responses in patients. However, the response rate remains below 30 %. In this study, we developed a polymeric bispecific antibody (BsAb) targeting PD1/PDL1 to enhance ICB therapy. Specifically, poly ($_L$-glutamic acid) (PGLU) was conjugated with a double cyclic Fc binding peptide, Fc-III-4C, through condensation reactions between the -COOH group of PGLU and the -NH_2 group of Fc-III-4C. This conjugate was then mixed with αPD1 and αPDL1 monoclonal antibodies (mAbs) in an aqueous solution. Mechanistically, the PD1/PDL1 BsAb ($BsAb_{αPD1+αPDL1}$) acts as a bridge between tumor cells and $CD8^+$ T cells, continuously activating $CD8^+$ T cells to a greater extent. This leads to significantly suppressed tumor growth and prolonged survival in a mouse model of colon cancer compared to treatment with either a single mAb or a mixture of free mAbs. The tumor suppression rate achieved by the $BsAb_{αPD1+αPDL1}$ was 90.1 %, with a corresponding survival rate of 83.3 % after 48 days. Thus, this study underscores the effectiveness of the $BsAb_{αPD1+αPDL1}$ as a synchronizing T cell engager and dual ICBs, offering theoretical guidance for clinical ICB therapy.

1. Introduction

In recent decades, immunotherapies, including checkpoint inhibitors, adoptive cell transfer, bispecific antibodies (BsAbs), monoclonal antibodies (mAbs), and vaccines, have emerged as efficient and highly specific treatments to combat cancer by enhancing the patient's immune response [1,2]. Notably, blocking coinhibitory immune checkpoints, such as the programmed cell death protein 1 (PD1; also known as CD279) antibody and its ligand PDL1 (also known as B7-H1 or CD274) antibody, has revolutionized cancer treatment by revitalizing T cells [3]. PD1, an inhibitory receptor found in T lymphocytes, interacts with its ligand PDL1, which is expressed in certain types of tumors [4–6]. Targeting the PD1/PDL1 coinhibitory pathway with monoclonal antibodies (mAbs) has led to durable tumor inhibition effects and approval for administration in various indications, including colon cancer, lung cancer, and melanoma [7–10]. By 2022, ten PD1 products (nivolumab, pembrolizumab, cemiplimab, sintilimab, camrelizumab, toripalimab, tislelizumab, zimberelimab, prolgolimab, and dostarlimab) and three PDL1 products (atezolizumab, durvalumab, and avelumab) have been approved for different cancer types since 2014 [11–14]. However, the response rates of anti-PD1 antibodies (αPD1) or anti-PDL1 antibodies (αPDL1) are approximately 20–30 % in patients with PDL1-positive tumors, indicating that the majority of cancer patients do not benefit from them [15–17]. Enhancing the response rate and therapeutic efficacy of PD1/PDL1-related therapy is therefore crucial.

Bispecific T cell engagers (BiTEs) are emerging and prominent bispecific antibodies (BsAbs) capable of binding spontaneously to both tumor antigens and T cells, effectively bridging these two entities. This interaction redirects and activates T cells, ultimately resulting in the targeted elimination of tumor cells [18,19]. Currently, several BiTEs are available on the market, including Blinatumomab (CD3 × CD19), Tebentafusp-tebn (CD3 × GP100), Mosunetuzumab (CD3 × CD20), and Teclistamab (CD3 × BCMA) [20–24]. BiTEs represent a significant portion of the BsAb pipeline in preclinical and clinical development,

* Corresponding author.
** Corresponding author.
*** Corresponding author.
E-mail addresses: liulinl@jlu.edu.cn (L. Liu), hujl100@nenu.edu.cn (J. Hu), nshen@ciac.ac.cn (N. Shen).

https://doi.org/10.1016/j.mtbio.2024.101239
Received 13 June 2024; Received in revised form 5 September 2024; Accepted 10 September 2024
Available online 14 September 2024

offering promising treatment prospects for various tumor types [25]. However, the primary production methods for BiTEs, such as the hybridoma approach and protein engineering technologies, are complex, involving a trial-and-error process that results in low yield, inconsistent quality, and significant impurities [26]. Given the maturity of monoclonal antibody (mAb) production technology, constructing BiTEs using a linker and well-established mAbs could offer a straightforward and efficient alternative, providing a new avenue for BiTE production.

Although most established BiTEs contain a fragment recognizing and activating CD3 on T cells, there is currently no CD3 monoclonal antibody available on the market for anti-tumor therapy. However, PD1 and PDL1 monoclonal antibodies (mAbs) are more accessible. PD1/PDL1 bispecific antibody ($BsAb_{\alpha PD1+\alpha PDL1}$) can bind to specific antigen epitopes on PD1-expressing T cells and highly expressed PDL1 on tumor cells, fostering the cytotoxic effect of T cells on PDL1-positive tumor cells. In this study, polymer-multiple Fc binding peptide conjugate (PGLU-Fc-III-4C) was synthesized by condensing the side –COOH of poly ($_L$-glutamic acid) (PGLU) with the $–NH_2$ of Fc-III-4C (a double cyclic peptide [27,28]). BsAb was then prepared by mixing PGLU-Fc-III-4C with αPD1 and αPDL1 mAbs (Scheme 1). The resulting $BsAb_{\alpha PD1+\alpha PDL1}$ acted as bridges between tumor cells and $CD8^+$ T cells, persistently activating $CD8^+$ T cells to a greater extent than a solution of free mixed mAbs. The preparation of $BsAb_{\alpha PD1+\alpha PDL1}$, its physiochemical properties, activation of $CD8^+$ T cells *in vitro*, subsequent induction of tumor cell death, tumor suppression, and the mechanism of $BsAb_{\alpha PD1+\alpha PDL1}$ were all verified. This strategy offers a novel and effective $BsAb_{\alpha PD1+\alpha PDL1}$, significantly enhancing the therapeutic efficacy of immune checkpoint blockade (ICB) therapies.

2. Material and methods

2.1. Materials

Fc-III-4C (amino acid sequence: NH_2-Cys-Asp-Cys-Ala-Trp-His-Leu-Gly-Glu-Leu-Val-Trp-Cys-Thr-Cys-COOH, two disulfide bonds form between Cys1-Cys4 and Cys2-Cys3) was procured from GL Biochem Ltd. (Shanghai, China). γ-Benzyl-$_L$-glutamate-N-carboxyanhydride (BLG-NCA) was obtained from Chengdu Enlai Biological Technology Co., Ltd. (Chengdu, China), purified by recrystallization from ethyl acetate, and vacuum-dried at room temperature before use. N,N-dimethylformamide (DMF) was acquired from Shanghai Haohong Scientific Co., Ltd. (Shanghai, China), dried over CaH_2 for 72 h, and distilled under reduced pressure prior to use. 1-Ethyl-3-(3-dimethylaminopropyl) carbodiimide hydrochloride (EDCI) and N-Hydroxy succinimide (NHS) were also sourced from Shanghai Haohong Scientific Co., Ltd. (Shanghai, China). Cy5-NH_2 was purchased from Wuhan Duofluor Inc. (Wuhan, China). Additionally, prestained Color Protein Molecular Weight Marker, Coomassie Blue Fast Staining Solution and BeyoGel™ Plus Precast PAGE Gel were purchased from Beyotime Biotechnology (Shanghai, China).

Anti-mouse PD1 antibody (αPD1, Rat IgG1, κ; Catalog: BE0146), anti-mouse PDL1 antibody (αPDL1, Rat IgG2b, κ; Catalog: BE0101) were procured from Bio X Cell (West Lebanon, NH, USA). Mouse IgG (Catalog: SP031) was obtained from Solarbio Science & Technology (Beijing, China). Fetal bovine serum (FBS) was sourced from Zhejiang Tianhang Biotechnology Co., Ltd., China. (Zhejiang, China). Penicillin and streptomycin were acquired from Huabei Pharmaceutical (Shijiazhuang, China). ELISA kits were purchased from Anoric.

2.2. Cells and animals

Murine colon cancer cell line MC38 was procured from Shanghai Bogoo Biotechnology Co. Ltd. (Shanghai, China). $CD8^+$ T cells for *in vitro* experiments were isolated from murine spleens. Spleens were meticulously removed, washed thrice with sterile PBS on ice, and gently fragmented using a syringe end before being filtered through 250-mesh nylon strainers. Red blood cells were lysed using Ammonium-Chloride-Potassium (ACK) Lysing Buffer (BioLegend). Subsequently, splenocytes were suspended in magnetic-activated cell sorting (MACS) buffer and

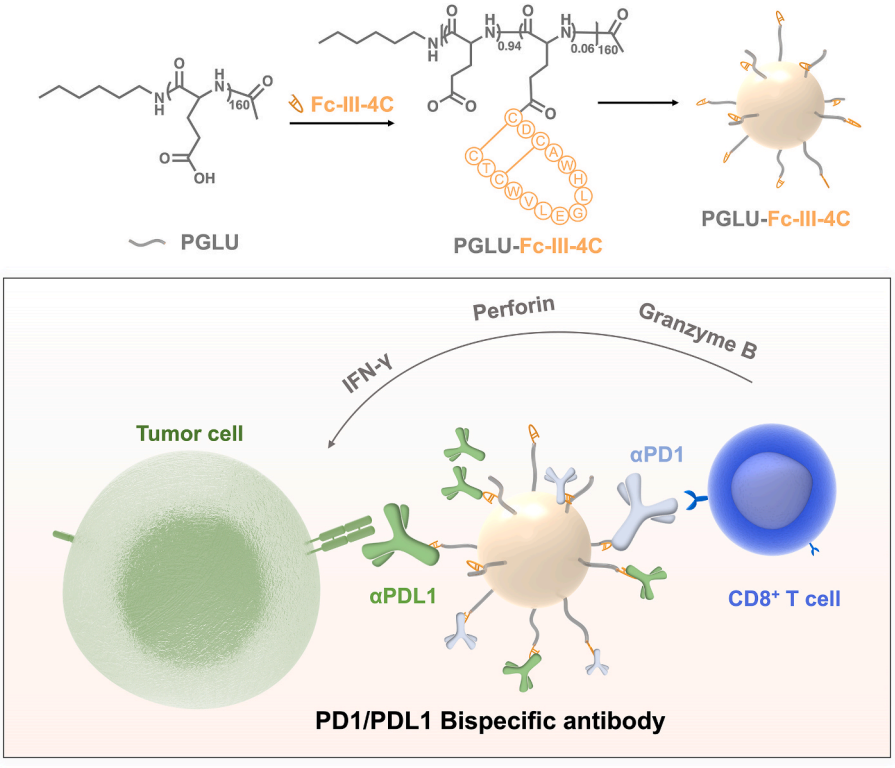

Scheme 1. $BsAb_{\alpha PD1+\alpha PDL1}$ simultaneously binds PD1 on the tumor cell and PDL1 on the $CD8^+$ T cell, engaging both cell types together while reinvigorating the $CD8^+$ T cells, further contributing to tumor cell death.

$CD8^+$ T cells were isolated using a CD8a (Ly2) microbeads Isolation Kit (Miltenyi Biotec.). For T cell stimulation, the isolated $CD8^+$ T cells were incubated with plate-bound anti-CD3 antibodies (5 μg/mL) and soluble anti-CD28 antibodies (5 μg/mL) for 48 h. The cells were cultured in RPMI 1640 medium with high glucose, supplemented with 10 % FBS, 1 % penicillin and 1 % streptomycin, and incubated at 37 °C in an atmosphere of 5 % CO_2 and 95 % air (approximately 20 % O_2 equivalent).

Female C57BL/6 mice were sourced from Beijing Vital River Laboratory Animal Technology Co., Ltd. (Beijing, China). The experimental animal procedures adhered to the guidelines outlined in the "Guide for Care and Use of Laboratory Animals" and received approval from the Animal Welfare and Ethics Committee of the Changchun Institute of Applied Chemistry, Chinese Academy of Sciences. The reference number for this approval is [CIAC-2023-0141].

2.3. Synthesis of PGLU

PGLU was synthesized by ring-opening polymerization of BLG-NCA, followed by deprotection. Briefly, BLG-NCA (10.0 g, 38 mmol) was dissolved in 100 mL of anhydrous DMF under a nitrogen atmosphere. Then, 1-hexylamine (24.0 mg, 0.2375 mmol), dissolved in 1.8 mL of anhydrous DMF, was added to initiate polymerization, which proceeded at 30 °C for 3 days. Subsequently, acetic anhydride (242 mg, 2.375 mmol) and triethylamine (240 mg, 2.375 mmol) were introduced, and the reaction continued for an additional 24 h at 30 °C. The resulting mixture was precipitated with an excess of ether to obtain poly(γ-benzyl L-glutamate) (PBLG) as a white solid. PBLG was next dissolved in 100 mL dichloroacetic acid, and 40 mL HBr/acetic acid (33 wt%) was added to facilitate deprotection. The solution was stirred at 30 °C for 1 h and subsequently precipitated with an excess of ether. The precipitate underwent dialysis against distilled water, and was subsequently lyophilized to yield PGLU with an 87 % yield.

2.4. Synthesis of PGLU-Fc-III-4C

Under anhydrous conditions, PGLU (10 mg, 0.3 μmol) and N,N′-disuccinimidyl carbonate (10.24 mg, 0.04 mmol) were dissolved completely in 10 mL DMF. Next, triethylamine (15 mg, 0.15 mol) was added to the mixture. The solution was then incubated at 37 °C for 48 h. Subsequently, Fc-III-4C (16 mg, 0.009 mmol) and an additional amount of triethylamine (10.2 mg, 0.1 mmol) were added. After another 2 h of incubation at 37 °C, the mixture solution was dialyzed sequentially against DMF and water. Finally, the solution was freeze-dried, resulting in the production of light-yellow powder with a yield of 42 %.

2.5. Synthesis of $NP_{\alpha PD1}$+$NP_{\alpha PDL1}$ and $BsAb_{\alpha PD1+\alpha PDL1}$

For the preparation of $NP_{\alpha PD1}$, a mixture comprising αPD1 and PGLU-Fc-III-4C was formulated at a precise mass ratio of 18.75:1, and a specified amount of PBS (0.01 M, pH 7.4) was added to dissolve the mixture. For $NP_{\alpha PD1}$, the mixture of αPD1 and PGLU-Fc-III-4C was prepared at a mass ratio of 18.75:1, too. $NP_{\alpha PD1}$+$NP_{\alpha PDL1}$ was achieved by mixing $NP_{\alpha PD1}$ and $NP_{\alpha PD1}$ in equal quantities. Each antibody in the solution was at a concentration of 1.0 mg/mL. Subsequently, the solution was incubated at 4 °C for 48 h. With the same preparation method, the mixture of αPD1, αPDL1, and PGLU-Fc-III-4C was prepared at a mass ratio of 18.75:18.75:1 The resulting products underwent direct measurements of molecular weight and size. To confirm whether PGLU-Fc-III-4C was linked to both monoclonal antibodies simultaneously, the solution was mixed with FITC-labeled anti-mouse PD1 antibody and PE/Cy7-labeled anti-mouse CD274 antibody to label αPD1 and αPDL1, respectively. The dual-color fluorescence of the solution was assessed using flow cytometry (BD FACS Celesta Multicolor Flow Cytometer, China).

2.6. Characterizations

The chemical structures of PGLU and PGLU-Fc-III-4C were analyzed using ^{1}H nuclear magnetic resonance spectroscopy (^{1}H NMR, Bruker, AV-300) with NaOD/D_2O as the solvent. Gel Permeation Chromatography (Waters GPC 3 system, Waters Ultra hydrogel Linear Column) was utilized to determine the molecular weight distribution and dispersion of PGLU, PGLU-Fc-III-4C, $BsAb_{\alpha PD1\&\alpha PDL1}$. Polyethylene glycol was employed as standards, with 0.2 M phosphate buffer (pH 7.4) as the eluting solvent. This test was conducted under 35 °C with the flow rate was 0.5 mL/min. The concentration of the sample is 2.0 mg/mL. All size measurements were performed with a Nano-Particle Analyzer (Malvern, Zetasizer Nano ZS, Shanghai Sibaiji Instrument System Co., LTD). TEM imaging was conducted using a JEOL JEM-1011 transmission electron microscope, located in Tokyo, Japan, operating at an accelerating voltage of 100 kV. 10 μL aqueous solution of nanoparticles (0.2 mg/mL) was dripped onto the copper net and TEM was performed after the water evaporated and dried. The molecular weight of αPD1, αPDL1 and $BsAb_{\alpha PD1+\alpha PDL1}$ were determined using asymmetric flow field-flow fractionation coupled with muti-angle laser light scattering (AF4-MALLS), conducted on a Wyatt Eclipse DualTec system (Dernbach, Germany). The system was equipped with a DAWN HELEOS-II (Santa Barbara, CA, USA), both operating at a wavelength of 658 nm. For these measurements, the refractive index increment of the samples in the eluent was assumed to be dn/dc = 0.185 mL/g. Data acquisition and analysis were performed using Wyatt Astra software.

2.7. Stability

PGLU-Fc-III-4C-IgG was synthesized following a previously published protocol. The mixture of IgG/PE-Cy7 and PGLU-Fc-III-4C was prepared at a mass ratio of 37.5:1, with an IgG/PE-Cy7 concentration of 37.5 μg/mL containing sodium azide (NaN_3, 1 μg/mL) in phosphate-buffered saline (PBS, 0.01 M, pH 7.4). The PGLU-Fc-III-4C-IgG/PE-Cy7 complex was incubated in human serum at a concentration of 9.5 mg/mL for 0 h, 8 h, 24 h, 48 h, and 72 h to assess its stability. The proportion of IgG/PE-Cy7 positive particles was analyzed using flow cytometry (BD FACS Celesta) to determine the stability of the complex over time.

2.8. Non-denaturing polyacrylamide gel electrophoresis

PGLU-Fc-III-4C-IgG was synthesized according to a previously established protocol. IgG and PGLU-Fc-III-4C were combined at a mass ratio of 37.5:1, with an IgG concentration of 1.0 mg/mL, and then incubated in PBS (0.01 M, pH 7.4) at 4 °C for 48 h. Subsequently, loading buffer was added, and the samples were boiled at 100 °C for 10 min. Non-denaturing polyacrylamide gel electrophoresis (PAGE) was conducted using an electrophoresis apparatus, followed by Coomassie Brilliant blue staining for 10 min. The gel was then shaken overnight in distilled water at 4 °C to remove excess stain, and visualization was performed using a gel imaging analyzer (Beijing Junyi Huaxin Technology Co., LTD., JY04S-3C, Beijing, China).

2.9. In vitro immune activation capability of $BsAb_{\alpha PD1+\alpha PDL1}$

MC38 cells were seeded at a density of 5×10^3 cells per well in 96-well plates and incubated overnight. 5×10^4 stimulated $CD8^+$ T cells were then added into each well and co-cultured with MC38 cells in 150 μL RPMI 1640 for another 24 h. 50 μL fresh RPMI 1640 medium containing mAbs, free mixed mAbs (αPD1+αPDL1), free mixed NPs ($NP_{\alpha PD1}$+$NP_{\alpha PDL1}$) or $BsAb_{\alpha PD1\&\alpha PDL1}$ was then added into wells. The concentration of mAbs was 20 μg/mL, and the $BsAb_{\alpha PD1+\alpha PDL1}$ had an equimolar of total antibodies to mAbs. After incubation at 37 °C and 5 % CO_2 for 6 h, cells were imaged using an optical microscope (Olympus, Japan). For another 48 h, tumor cells were analyzed by CCK-8 assay and supernatants were subjected to IFN-γ, perforin, and granzyme B analysis

by ELISA kit according to the manufacturer's instructions.

2.10. In vivo anti-tumor study

MC38 tumor models were established by subcutaneous injecting 1.0 × 10^6 MC38 cells to the right flank of C57BL/6 mice (female, 6 weeks old, 20 g). When tumor volumes reached around 80–100 mm^3, the mice were divided into 6 groups randomly with 6 mice per group, and treated with: PBS, αPD1, αPDL1, $Free_{αPD1+αPDL1}$, $NP_{αPD1}$+$NP_{αPDL1}$ and $BsAb_{αPD1+αPDL1}$. All treatments are performed by intravenous (i.v.) injection with 200 μL PBS as solvent on day 0, 2, 4, 7.

Long and short tumor diameters were measured using a caliper, and the body weight was measured and recorded every 2 days. The volumes of the tumor were calculated using the formula for mouse tumor calculation: $V = (a \times b^2)/2$, where "a" represents the longest diameter of the tumor and "b" is the shortest diameter. The Tumor inhibition rate (TSR) was determined by the following formula: TSR (%) = [(Vc - Vt)/Vc] × 100 %, with Vc being the average tumor volume of the control group, and Vt the average tumor volume of the treatment group (PBS). The survival rate of the mice was monitored every other day. The mice with tumors larger than 2000 mm^3 were considered dead.

To establish a bilateral tumor model, When the primary tumor on the right reached approximately 100 mm^3 and the secondary tumors on the left (as the secondary tumor) reached approximately 50 mm^3, mice were randomly divided into six groups: PBS, αPD1, αPDL1, $Free_{αPD1+αPDL1}$, $NP_{αPD1}$+$NP_{αPDL1}$ and $BsAb_{αPD1+αPDL1}$. All treatments are performed by intravenous (i.v.) injection with 200 μL PBS as solvent on day 0, 2, 4, 7.

2.11. Biodistribution and pharmacokinetics analyses

Under anhydrous conditions, PGLU (10 mg) and N,N′-disuccinimidyl carbonate (10.24 mg, 0.04 mmol) were dissolved completely in 10 mL DMF. Next, triethylamine (15 mg, 0.15 mol) was added to the mixture. The solution was then incubated at 37 °C for 48 h. Fc-III-4C (16 mg, 0.009 mmol) was added for another 2 h at 37 °C in dark. Subsequently, Cy5-NH_2 (3 mg, 0.005 mmol) was added for another 12 h at a room temperature in dark. This solution was transferred into a dialysis bag (MWCO = 5000 Da, Mengyimei Biotechnology Co., LTD, Beijing, China) and dialyzed against water for 72 h. After freeze-drying, a blue solid, Cy5-labeled PGLU (PGLU/Cy5) was obtained with a yield of 96.6 %. Next, PGLU-Fc-III-4C/Cy5, $NP_{αPD1}$+$NP_{αPDL1}$/Cy5 and $BsAb_{αPD1+αPDL1}$/Cy5 were prepared according to the previous method.

MC38 tumor models were established via the subcutaneous injection of 1.0 × 10^6 MC38 cells to the right flank of C57BL/6 mice (female, 6 weeks old, 20 g). When the tumor had reached approximately 300–500 mm^3, mice were randomly allocated into three groups of 3 mice per group and treated with: Cy5-labed PGLU-Fc-III-4C-IgG, $NP_{αPD1}$+$NP_{αPDL1}$ and $BsAb_{αPD1+αPDL1}$ by intravenous (i.v.) with 200 μL PBS as solvent. 24 h after post-administration, the tumors and normal organs were harvested and the biodistribution of nanoparticles was visualized using an IVIS Lumina LT Seres III *in vivo* imaging system.

The pharmacokinetics of IgG, PGLU-Fc-III-4C-IgG and $BsAb_{αPD1+αPDL1}$ were assessed by the fluorescence intensity of Cy5 in the serum at various time points after the intravenous injection of different drugs into rats (n = 3).

2.12. Immune analysis

Flow cytometry assay was performed to analyze immune cells infiltrated in tumor. The subcutaneous MC38 tumor model, the grouping of tumor-bearing mice, and the way of drug administration are the same as those *in vitro* antitumor experiments. On day 9 in the tumor inhibition experiment of treatment, the mice were sacrificed, and both the tumor and spleen were collected. These tissues were gently grinded and strained through 250-μm nylon strainers to produce single cell suspensions. The single-cell suspensions were then washed with PBS (0.01 M, pH 7.4) supplemented with 2 % FBS. Subsequently, the cells were stained with a panel of fluorescent dyes conjugated to anti-mouse antibodies specific for CD3, CD4 and CD8 markers, followed by fixation with 4 % paraformaldehyde. The presence and distribution of T lymphocytes within the tumor and spleen tissues were detected and analyzed using flow cytometry (BD FACS Celesta).

2.13. Cytokine analysis

Peripheral blood was collected from mice 48 h after treat by different drugs and centrifuged at 1000×*g* at 4 °C for 15 min within 30 min of collection. The concentrations of the cytokines (IFN-γ, TNF-α and IL-12) in serum were then measured using ELISA kit according to the manufacturer's instructions.

2.14. Hematoxylin and eosin (H&E) staining

MC38 tumor models were established by subcutaneous injection of 1.0 × 10^6 MC38 cells to the right flank of C57BL/6 mice (female, 6 weeks old, 20 g). Mice bearing a unilateral MC38 tumor were treated with PBS, $NP_{αPD1}$+$NP_{αPDL1}$ and $BsAb_{αPD1+αPDL1}$ (n = 3 per group) administered by intravenous (i.v.) injection with 200 μL PBS as solvent on days 0, 2, 4, and 7. Mice were euthanized on day 13, and major organs including heart, liver, spleen, lung and kidney were excised. Those organs were then fixed in 4 % buffered paraformaldehyde overnight and subsequently embedded in paraffin. Tissue sections of 5 μm thickness were prepared and stained with hematoxylin and eosin for histopathological analysis, which was conducted under a light microscope (Nikon TE2000U).

2.15. Systemic toxicity

Groups of three mice each were intravenously administered with αPD1, αPDL1, $Free_{αPD1+αPDL1}$, $NP_{αPD1}$+$NP_{αPDL1}$ and $BsAb_{αPD1+αPDL1}$. Nine days post-injection, blood samples were collected and centrifuged at 3000 rmp for 5 min to isolate plasma. The plasma was then analyzed using an automated biochemical analyzer to measure liver and kidney function parameters such as alanine aminotransferase (ALT), aspartate aminotransferase (AST), alkaline phosphatase (AKP), blood urea nitrogen (BUN), creatinine (CRE) and uric acid (UA).

2.16. Statistical analysis

All experiments were conducted with a minimum of two repetitions, and the results are presented as mean values ± standard deviation (SD). Statistical analysis for multiple group comparisons was performed using one-way ANOVA followed by Tukey's multiple comparison. Unpaired student's t-test was used for statistical analysis in experiments with two groups of data. "ns" means no significance. Survival differences were determined using Kaplan-Meier analysis, with the overall significance determined by og-rank test. $^*p < 0.05$ was considered statistically significant, while $^{**}p < 0.01$ and $^{***}p < 0.001$ were considered highly and extremely levels of significant, respectively. *p* values were annotated on the figures. The figure legend detail the number of animals included in each study.

3. Results and discussion

3.1. Synthesis and characterization of the carrier polymer PGLU-Fc-III-4C

The carrier polymer contains a backbone of PGLU and multiple grafts of Fc-III-4C peptide. PGLU is a biocompatible and biodegradable polymer, with various downstream being tested in clinical trials. Fc-III-4C is an artificially synthesized 15-amino acid double cyclic peptide mimicking the Z-domain of Protein A, and it binds to the IgG Fc region

with high affinity (dissociation constant (K_D): K_D = 2.45 nM to human IgG and 12.3 nM for mouse IgG) [29,30]. The PGLU, PGLU-Fc-III-4C were similarly synthesized as our previous works [31–33]. PGLU was synthesized via the ring-opening polymerization of γ-benzyl-$_L$-glutamate N-carboxyanhydride, which was subsequently followed by the removal of the γ-benzyl protecting groups [31,34]. The Fc-III-4Cs were attached to PGLU molecular chains by a condensation reaction between the terminal amino groups and the side carboxyl groups of PGLU (Fig. S1). The PGLU-Fc-III-4C contained a chain of 160 $_L$-glutamic acid residues as depicted in Figure S2. Sulfur element analysis revealed a 3.9 % sulfur content in PGLU-Fc-III-4C, with the side chains of $_L$-glutamic acid (Glu) present as sodium salts (Table S2). This data coupled with the integration of areas and structural hydrogen numbers of δ 6.69–7.73 ppm (h, i) in the ^{1}H NMR spectrum (Fig. S2), confirmed that each PGLU-Fc-III-4C molecule contained an average of 13.6 Fc-III-4C grafts.

3.2. Bispecific antibody ($BsAb_{\alpha PD1+\alpha PDL1}$)

Tumor cells frequently overexpress these immune checkpoint proteins as a strategy to evade detection and destruction by the host immune system, effectively suppressing T-cell-mediated tumor rejection [35–38]. Preclinical and clinical evidence has demonstrated that antibody blockade of immune checkpoints can significantly augment enhance antitumor immunity, with combined administration proven to intensify T-cell activation in the context of immunotherapy [39,40]. They were selected as two representative mAbs for $BsAb_{\alpha PD1+\alpha PDL1}$ preparation with PGLU-Fc-III-4C. A 1:1 αPD1 to αPDL1 molar ratio was taken. The PGLU-Fc-III-4C was incubated with $Free_{\alpha PD1+\alpha PDL1}$ in PBS (Fig. 1A). As shown by Fig. 1D, DLS results showed that free αPD1 and αPDL1 had an average hydrodynamic diameter of 11.3 ± 0.8 nm and 13.5 ± 0.6 nm, respectively. The $Free_{\alpha PD1+\alpha PDL1}$ show a hydrodynamic diameter of 19.3 ± 3.4 nm, while the PGLU-Fc-III-4C's hydrodynamic diameter is 43.8 ± 1.7 nm. The $BsAb_{\alpha PD1+\alpha PDL1}$ exhibited a substantially enhanced diameter of 112.3 ± 1.9 nm which without purification. The diameters determined by DLS experiments was in agreement with those observed via transmission electron microscopy (TEM) for $BsAb_{\alpha PD1+\alpha PDL1}$ with an average diameter of 88.3 ± 15.9 nm as shown in Fig. 1B. In contrast, PGLU-Fc-III-4C-IgG exhibited a profile that negated

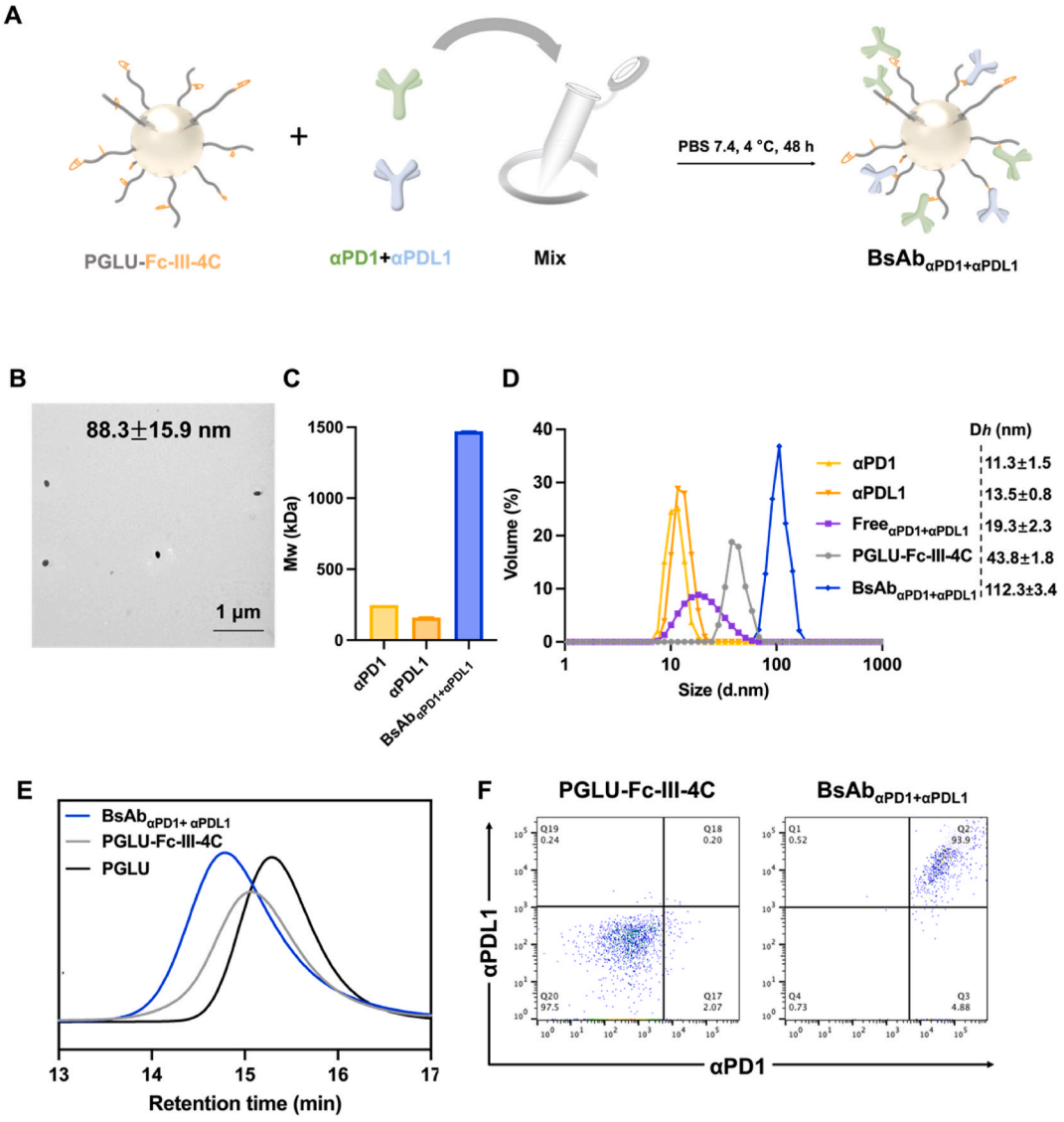

Fig. 1. Synthesis and characterization of $BsAb_{\alpha PD1+\alpha PDL1}$. (A) Schematic representation and preparation of $BsAb_{\alpha PD1+\alpha PDL1}$. (B) Transmission electron microscopy (TEM) images of $BsAb_{\alpha PD1+\alpha PDL1}$ (Scale bar: 1 μm). (C) Molecular weight of αPD1, αPDL1 and $BsAb_{\alpha PD1+\alpha PDL1}$, as measured by asymmetric flow field-flow fractionation coupled with multiangle laser light scattering. (D) Particle size of PGLU-Fc-III-4C and $BsAb_{\alpha PD1+\alpha PDL1}$, as detected by DLS. Average diameters for each sample are shown. (E) The molecular weights of PGLU, PGLU-Fc-III-4C, $BsAb_{\alpha PD1+\alpha PDL1}$ were measured with Gel Permeation Chromatography (GPC). (F) Flow cytometric analysis detecting FITC labeled anti-PD1 and PE-Cy7 labeled anti-PDL1 antibodies conjugated into a $BsAb_{\alpha PD1+\alpha PDL1}$.

the need for purification, which was corroborated by nondenaturing polyacrylamide gel electrophoresis, followed by Coomassie blue staining, as depicted in Figure S3. As illustrated in Fig. 1E and Table S1, the elution time of $BsAb_{\alpha PD1+\alpha PDL1}$ was earlier than that of PGLU-Fc-III-4C and PGLU, suggesting that the $BsAb_{\alpha PD1+\alpha PDL1}$ possesses a significantly larger mass compared to PGLU-Fc-III-4C and PGLU.

The expression of PDL1 on MC38 was analyzed by flow cytometry (Fig. S4). The mixture of αPD1 and αPDL1 was labeled with FITC and PE-Cy7, respectively, and then subjected to two-color fluorescence detection with flow cytometry. Nearly all particles of $BsAb_{\alpha PD1+\alpha PDL1}$ (93.9 %) and PGLU-Fc-III-4C (97.5 %) were respectively categorized into double-positive and double-negative gates, indicating of the dual fluorescent labeling on PGLU-Fc-III-4C and the effective construction of $BsAb_{\alpha PD1+\alpha PDL1}$ (Fig. 1F). Based on the average weight mass (Mw) determined by static light scattering detector (Fig. 1C), and the inputted Mw ratio of αPD1+αPDL1 and PGLU-Fc-III-4C is 37.5:1. It is theoretically deduced that the 1470 kDa $BsAb_{\alpha PD1+\alpha PDL1}$ consisted of 42.4 kDa from PGLU-Fc-III-4C and 1427.6 kDa from antibodies (αPD1+αPDL1). Assuming the Mw of αPD1 and αPDL1 to be 247.7 kDa and 159.7 kDa, respectively. Each $BsAb_{\alpha PD1+\alpha PDL1}$ were bound an average of 7.0 total antibodies at the 1:1 of the αPD1: αPDL1 input molar ratio. These results demonstrate the high binding ability of the Fc-III-4C grafts as well as the multivalent characteristics of the obtained $BsAb_{\alpha PD1+\alpha PDL1}$.

3.3. *The T cell-activation ability of $BsAb_{\alpha PD1+\alpha PDL1}$*

The stability of PGLU-Fc-III-4C-IgG was monitored over a period of 72 h in IgG-stimulated blood environment (9.6 g/L IgG), and it exhibited no significant alterations. The percentage of IgG-PE-Cy7 conjugated PGLU-Fc-III-4C was maintain a level above 91.0 % (Fig. 2A–B). This finding demonstrated that $BsAb_{\alpha PD1+\alpha PDL1}$ could be stable in mice for about three days.

MC38 tumor cells were incubated with $CD8^+$ T cells in medium containing $Free_{\alpha PD1+\alpha PDL1}$, $NP_{\alpha PD1}$+$NP_{\alpha PDL1}$ or $BsAb_{\alpha PD1+\alpha PDL1}$. Then

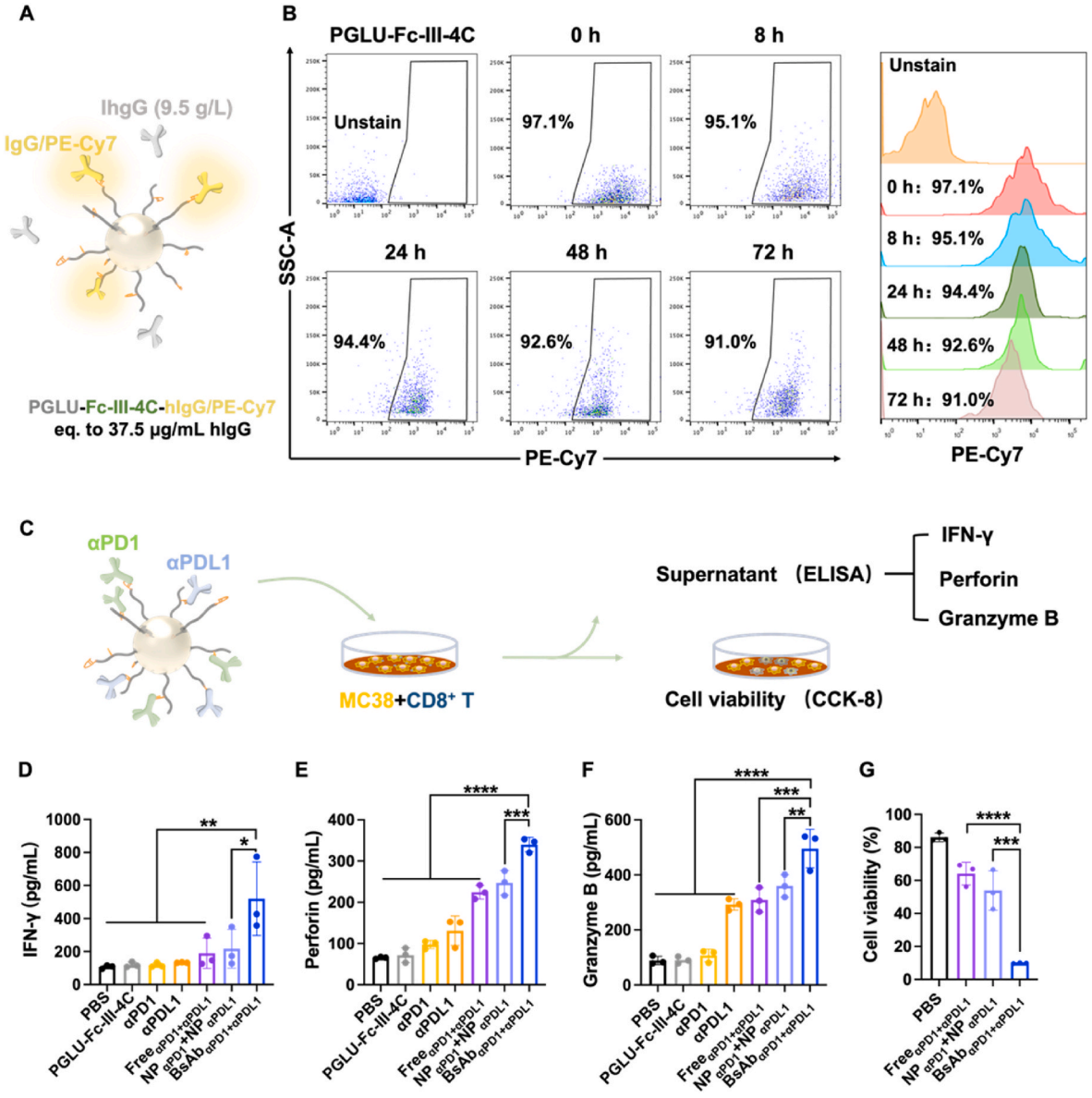

Fig. 2. *In vitro* stability testing, tumor inhibition and $CD8^+$ T cell activation activity of $BsAb_{\alpha PD1+\alpha PDL1}$. (A) Schematic representation of the experimental of stability testing. (B) Flow cytometry analysis detecting the stimulative stability of PGLU-Fc-III-4C-hIgG-PE-Cy7 in human blood in 72 h, in which the hIgG was 9.5 g/L. PGLU-Fc-III-4C without hIgG-PE-Cy7 was used as a control for gating. (C) Schematic representation of the experimental process assessing *in vitro* activity of $BsAb_{\alpha PD1+\alpha PDL1}$ in a co-culture of MC38 cells and $CD8^+$ T cells. (D–F) IFN-γ, perforin, and granzyme B ELISA results from supernatants of co-cultured MC38 cells and $CD8^+$ T cells at 24 h after treatment. (G) CCK-8 assay detecting different drugs induced anti-tumor effect of $CD8^+$ T cells.

cytokine production was subsequently analyzed 24 h after coincubation. When compared with equivalent dosage of non-conjugated mix mAbs ($Free_{\alpha PD1+\alpha PDL1}$), the $BsAb_{\alpha PD1+\alpha PDL1}$ stimulated significantly higher level of interferon-gamma (IFN-γ), perforin and granzyme B (Fig. 2D–F). These cytokines are crucial for mediating the immune response of cytotoxic T lymphocyte [41,42]. Moreover, the $Free_{\alpha PD1+\alpha PDL1}$ only kill ~33 % MC38 cancer cells, the $NP_{\alpha PD1}$+$NP_{\alpha PDL1}$ could kill ~46 % MC38 cells, while the $BsAb_{\alpha PD1+\alpha PDL1}$ killed ~90 % MC38 cells (Fig. 2G). These results demonstrate the $BsAb_{\alpha PD1+\alpha PDL1}$ has superior T-cell activation ability and tumor cell killing ability than the free antibody mixture.

3.4. The antitumor ability of $BsAb_{\alpha PD1+\alpha PDL1}$

As shown in Fig. 3A, optical images illustrated that in the $BsAb_{\alpha PD1+\alpha PDL1}$ group, $CD8^+$ T cells were mostly found in close proximity to adherent MC38 cells. $BsAb_{\alpha PD1+\alpha PDL1}$ exhibits superior efficacy to active T-cell and subsequent eliminating tumor cells compared to a mixture of free mAbs.

According to the positive results of the cytokine analyses and the optical images *in vitro*, we tried to evaluate $BsAb_{\alpha PD1+\alpha PDL1}$ antitumor efficacy *in vivo*. To assesses $BsAb_{\alpha PD1+\alpha PDL1}$ antitumor efficacy, imaging experiments were performed in mice. As depicted in Fig. 3B, *in vivo* imaging showed that $BsAb_{\alpha PD1+\alpha PDL1}$ exhibited a significantly enhanced distribution compared to those of $NP_{\alpha PD1}$+$NP_{\alpha PDL1}$ and $BsAb_{\alpha PD1+\alpha PDL1}$, corroborating the targeting capabilities of αPDL1. The *ex vivo* imaging obtained the same results. And the pharmacokinetic results (Fig. S7) showed that $BsAb_{\alpha PD1+\alpha PDL1}$ showed a considerably prolonged blood circulation time ($t_{1/2}$ = 20.1 ± 4.4 h) compared to IgG ($t_{1/2}$ = 10.1 ± 1.7 h), which proving that structure and characteristics of $BsAb_{\alpha PD1+\alpha PDL1}$ did not affect the circulation time compared with PGLU-Fc-III-4C-IgG ($t_{1/2}$ = 19.8 ± 1.1 h).

Subsequently, we aimed to determine whether $BsAb_{\alpha PD1+\alpha PDL1}$ could elicit an enhanced antitumor effect *in vivo* compared to the mixture of NPs ($NP_{\alpha PD1}$+$NP_{\alpha PDL1}$). PDL1 receptors are expressed on MC38 tumor cells (Figure S5). Fig. 4A show the set groups and the corresponding administration methods. Fig. 4B shows the tumor growth rate. In Groups 2 and 3, the administered concentrations of αPD1 and αPDL1 were 2.5 mg/kg, respectively. For Group 4, the concentration of the free antibody mixture was 5.0 mg/kg. In Group 5, the total administered concentration of $NP_{\alpha PD1}$+$NP_{\alpha PDL1}$ was 5.27 mg/kg, comprising 5.0 mg/kg of antibodies and 0.27 mg/kg of the PGLU-Fc-III-4C conjugate. The PBS control group show fast tumor growth. The single αPD1, αPDL1, $Free_{\alpha PD1+\alpha PDL1}$ and $NP_{\alpha PD1}$+$NP_{\alpha PDL1}$ all show relatively slower tumor growth rate, indicating the tumor growth suppression effects of each drug. The $BsAb_{\alpha PD1+\alpha PDL1}$ shows even improved tumor growth suppression effect than the simple antibody NPs mixture. Specifically, the

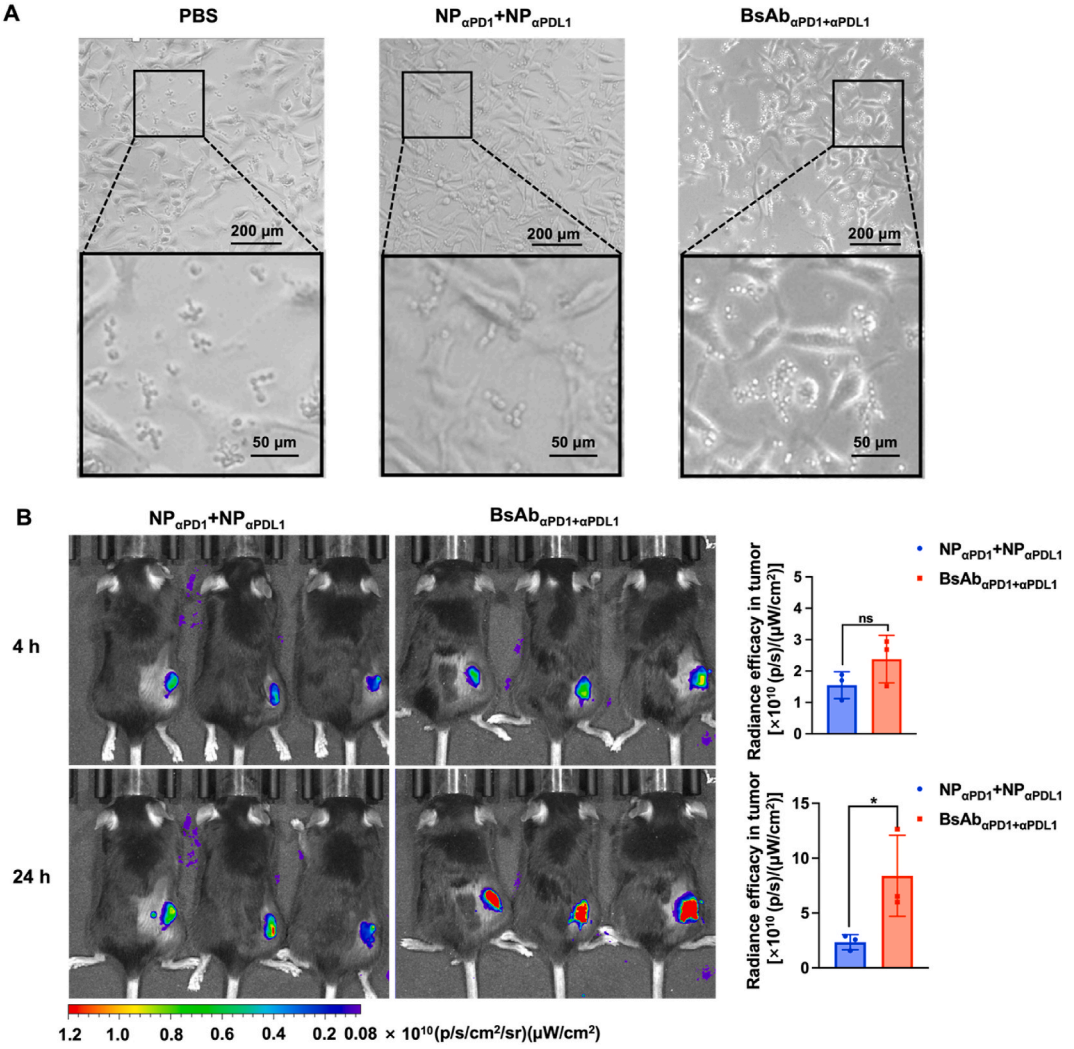

Fig. 3. (A) Optical microscope photographs of the cocultured MC38 and $CD8^+$ T cells at 6 h after treatment with PBS, $NP_{\alpha PD1}$+$NP_{\alpha PD1}$ and $BsAb_{\alpha PD1+\alpha PDL1}$. *In vivo* biodistribution of Cy5-labeled $NP_{\alpha PD1}$+$NP_{\alpha PD1}$ and $BsAb_{\alpha PD1+\alpha PDL1}$. (B) *In vivo* fluorescent imaging of drug distribution in mice at 4 h and 24 h post-injection and quantitative analysis of the fluorescence in the tumor (n = 3 mice/group).

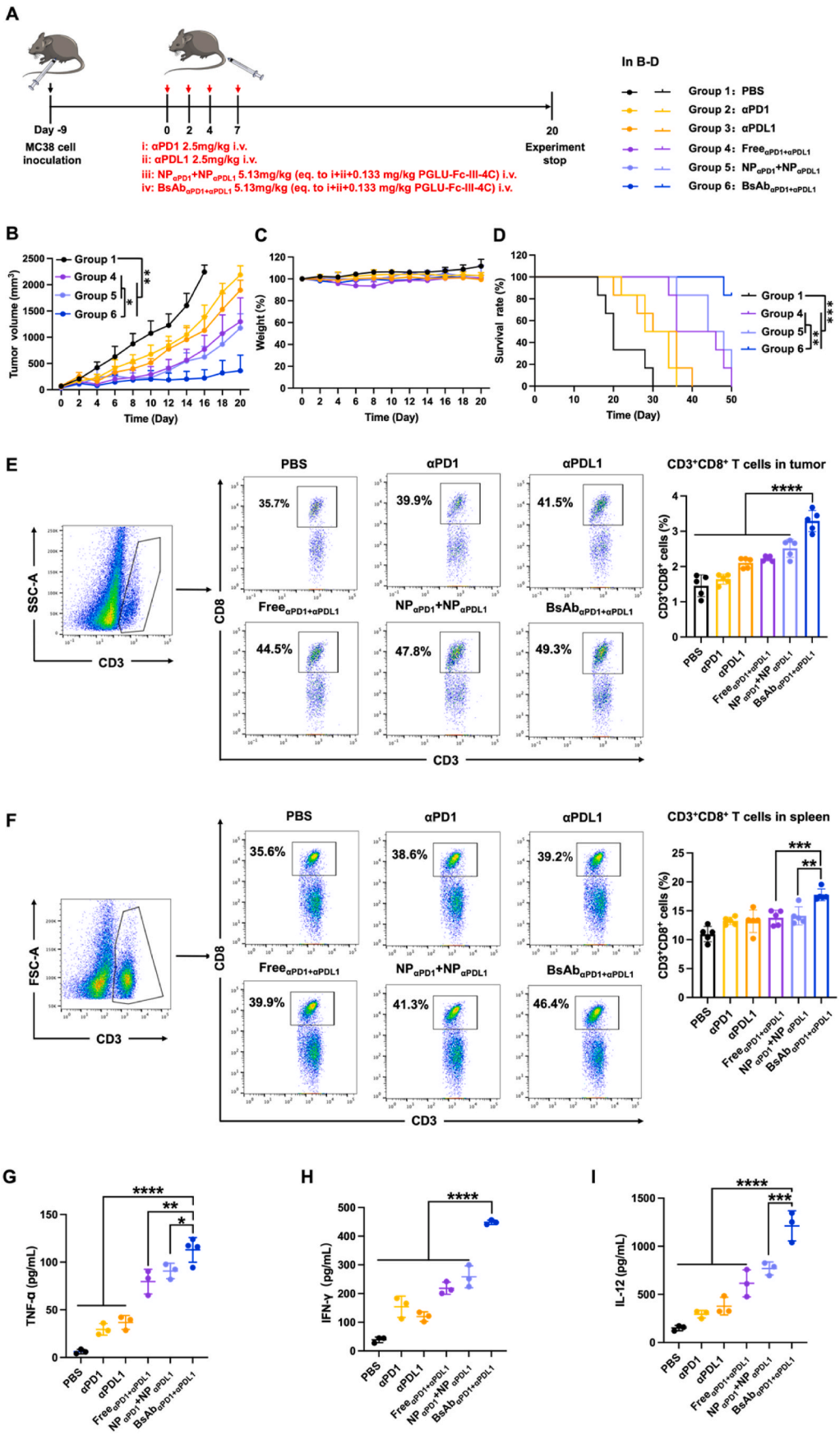

(caption on next page)

Fig. 4. A) Schedule for drug treatment in the tumor inhibition experiment. (B) Tumor growth curve, (C) body weight change, and (D) survival curve for mice after different treatments (n = 6 mice/group). (E) Flow cytometry analyzing $CD8^+$ T cells levels at day 9 in the tumor inhibition experiment. (F) Flow cytometry analyzing $CD8^+$ T cells levels at day 9 in the spleen inhibition experiment (n = 5 mice/group). (G–I) Serum cytokine levels were detected by ELISA assay, including (G) IFN-γ, (H) TNF-α and (I) IL-12 (n = 3 mice/group).

tumor suppression rate (TSR) of the mixture of two NPs was 72.3 %, while that of the $BsAb_{αPD1+αPDL1}$ group was 90.1 % on day 16, proving that the $BsAb_{αPD1+αPDL1}$ effectively boost the efficacy of combination immunotherapy. Fig. 4C shows the fluctuations in body weight observed in mice. At the initial stage of the treatments, the mice in experimental treatment group $Free_{αPD1+αPDL1}$ showed slightly body weight loss. After 8 days, the body weight of the treatment group of $Free_{αPD1+αPDL1}$ mice returned to normal.

Fig. 4D shows the survival curve of the mice. In Group $BsAb_{αPD1+αPDL1}$, the survival time of the mice in is significantly prolonged. Compared with PBS. After 48 days, the STR of the Group $BsAb_{αPD1+αPDL1}$ is 83.3 %, while the STR of mice in all the other groups is below 35 %. These results prove that the $BsAb_{αPD1+αPDL1}$ can effectively prolong the survival period of tumor-bearing mice in MC38 model of primary colon cancer. In view of the improved tumor suppressor effect and the well-tolerated condition of mice, the $BsAb_{αPD1+αPDL1}$ finally significantly prolonged the survival period of mice with lower toxic and side effects. In bilateral tumor model (Fig. S9), both the PD1 group and the PDL1 group demonstrated moderate tumor suppression effects for primary tumors, with a TSR of 42.0 % and 55.6 %, respectively. The TSR of $Free_{αPD1+αPDL1}$ and $NP_{αPD1}$+$NP_{αPDL1}$ group were 66.6 % and 65.6 %, respectively. Importantly, the group of $BsAb_{αPD1+αPDL1}$ significantly

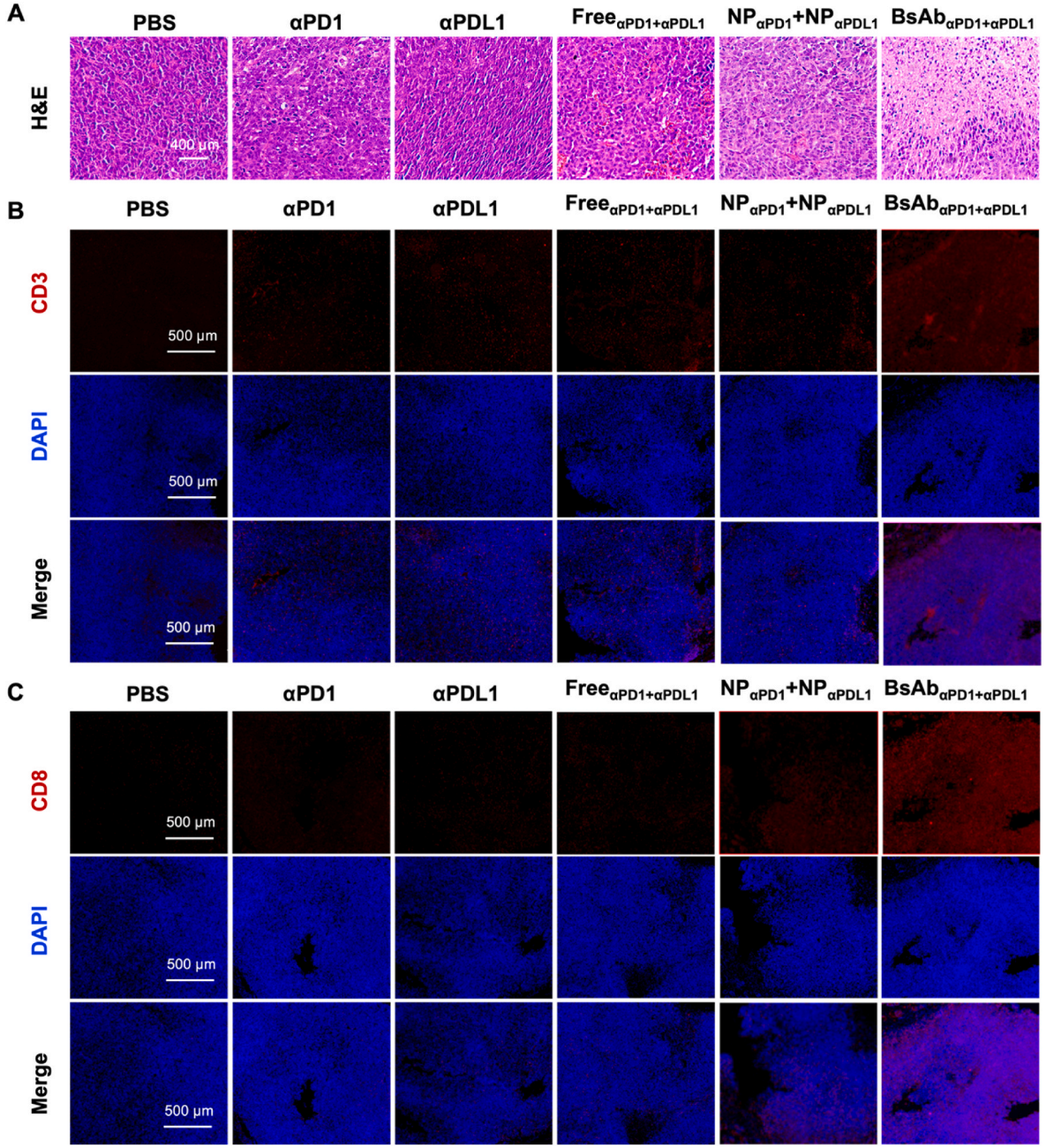

Fig. 5. H&E staining of tumors (Scale bar: 400 μm) and representative immunofluorescence images of tumors (Scale bar: 500 μm) after $BsAb_{αPD1+αPDL1}$ treatment.

suppressed primary tumor growth (TSR = 87.0 %). These results indicate that the $BsAb_{\alpha PD1+\alpha PDL1}$ effectively inhibits primary tumor growth. In line with the observed inhibition of primary tumor growth, $BsAb_{\alpha PD1+\alpha PDL1}$ group also markedly suppressed secondary tumor growth (TSR = 83.3 %), whereas other treatment groups did not exhibit a substantial suppression of secondary tumor growth (Fig. S9). Furthermore, no significant weight loss was noted in any group of mice during the observation period, underscoring the safety of the treatment regimen (Fig. 4C).

To analyze the tumor growth inhibiting mechanism of $BsAb_{\alpha PD1+\alpha PDL1}$, we further evaluated the immune cell infiltration and representative immunofluorescence images of tumors and spleens after various treatments. T cells play a role in killing tumors and inhibiting tumor growth in the immune response [43,44]. As depicted in Fig. 4E–F, the up-regulation of $CD8^+$ T cells of Group $BsAb_{\alpha PD1+\alpha PDL1}$ proved that. The IFN-γ, TNF-α and IL-12's expression levels were also detected with ELISA kits (Fig. 4G–I). These cytokines play important roles in inhibiting tumor growth. The activated $CD8^+$ T cells are capable of secreting IFN-γ and TNF-α, which can inhibit the formation of tumor blood vessels. IL-12, a cytokine regulated by IFN-γ, plays a crucial role in the activation of natural killer (NK) cells. TNF-α can also kill or inhibit the proliferation of tumor cells, and improve the ability of T cells and other killer cells to kill tumor cells [45]. After the treatment with the $BsAb_{\alpha PD1+\alpha PDL1}$ prepared in the work, the expressions of IFN-γ, TNF-α and IL-12 were all up-regulated, indicating that the $BsAb_{\alpha PD1+\alpha PDL1}$ can trigger both adaptive and innate immune responses, which probably significantly led to the inhibition of the growth and development of mouse colon tumors and the prolonging of the survival time of tumor-bearing mice.

To further evaluate the therapeutic effect, we performed immunofluorescent labeling of the resected tumor to observe the presence of $CD3^+$ T cells in the tumor tissue. The strongest red fluorescence ($CD3^+$ T and $CD8^+$ T cells) can be seen in the tumors after $BsAb_{\alpha PD1+\alpha PDL1}$ treatment, indicating that the tumor cells in the treatment group had the most T cells (Fig. 5B–C). H&E sections also observed more bad colored tumor cells (Fig. 5A), demonstrating that large areas of necrosis occurred within the tumor after BsAb treatment, while no significant changes were observed in normal organs [46]. The serum levels of BUN, ALT, AST, AKP, CRE and UA all exhibited similar levels across experimental groups (Fig. S8). This indicating that the treatment of $BsAb_{\alpha PD1+\alpha PDL1}$ did not adversely impact liver and kidney function. Furthermore, consistent with the results so far, no significant pathological alterations were detected in the heart, liver, spleen, lung and kidney in any of the treatment groups, as detailed in Fig. S6. In tumor, more tumor cell apoptosis was seen in the $BsAb_{\alpha PD1+\alpha PDL1}$ group compared with the PBS group. The results demonstrated that $BsAb_{\alpha PD1+\alpha PDL1}$ was safe and effective, with stronger killing effect on tumor cells.

4. Conclusion

In summary, we propose a novel strategy to enhance immune checkpoint blockade therapy using polymeric PD1/PDL1 bispecific antibodies ($BsAb_{\alpha PD1+\alpha PDL1}$). The desired $BsAb_{\alpha PD1+\alpha PDL1}$ was constructed by gently mixing a polymer-multiple Fc binding peptides with αPD1 and αPDL1 monoclonal antibodies (mAbs) in an aqueous solution. Furthermore, it acts as an innovative T cell engager, stimulating immune activation, tumor cell elimination, inhibition of tumor growth, and prolonged survival. *In vivo* imaging and dissection experiments demonstrated that $BsAb_{\alpha PD1+\alpha PDL1}$ exhibited significantly enhanced distribution compared to $NP_{\alpha PD1}$+$NP_{\alpha PDL1}$ and $BsAb_{\alpha PD1+\alpha PDL1}$, attributed to the targeting ability of αPDL1. H&E staining analysis revealed no significant pathological abnormalities in the major organs of mice treated with $BsAb_{\alpha PD1+\alpha PDL1}$. The up-regulation of anti-tumor cytokines indicates that $BsAb_{\alpha PD1+\alpha PDL1}$ can induce the activation of adaptive and innate immunity, likely contributing to the inhibition of mouse colon tumor growth and prolonged survival in tumor-bearing mice. $BsAb_{\alpha PD1+\alpha PDL1}$ demonstrated favorable therapeutic efficacy and enhanced anti-tumor immune responses compared to free mAbs alone, highlighting its interactions and collaborative functions. This study provides new insights into strategies for enhancing clinical immune checkpoint blockade therapy.

CRediT authorship contribution statement

Fuxin Xue: Writing – original draft, Formal analysis, Data curation. **Xitong Ren:** Methodology. **Chaoying Kong:** Methodology. **Jianfeng Wang:** Methodology. **Linlin Liu:** Supervision. **Junli Hu:** Supervision. **Na Shen:** Conceptualization, Project administration, Supervision, Writing – review & editing, Data validity, Funding acquisition. **Zhaohui Tang:** Funding acquisition.

Declaration of competing interest

The authors declare that they have no known competing financial interests or personal relationships that could have appeared to influence the work reported in this paper.

Data availability

Data will be made available on request.

Acknowledgements

This work is financially supported by the the Jilin province, China (20230508102RC), Ministry of Science and Technology of China (2022YFE0110200), National Natural Science Foundation of China (52273157, 52073279, 52025035), as well as the Youth Innovation Promotion Association of Chinese Academy of Sciences, China (2022224).

Appendix B. Supplementary data

Supplementary data to this article can be found online at https://doi.org/10.1016/j.mtbio.2024.101239.

References

[1] J.L. Adams, J. Smothers, R. Srinivasan, Big opportunities for small molecules in immuno-oncology, Nat. Rev. Drug Discov. 14 (2015) 603–622, https://doi.org/10.1038/nrd4596.
[2] Y. Zhang, Z. Zhang, The history and advances in cancer immunotherapy: understanding the characteristics of tumor-infiltrating immune cells and their therapeutic implications, Cell. Mol. Immunol. 17 (2020) 807–821, https://doi.org/10.1038/s41423-020-0488-6.
[3] C. Robert, A decade of immune-checkpoint inhibitors in cancer therapy, Nat. Commun. 11 (2020) 3801, https://doi.org/10.1038/s41467-020-17670-y.
[4] S.P. Kubli, T. Berger, D.V. Araujo, L.L. Siu, T.W. Mak, Beyond immune checkpoint blockade: emerging immunological strategies, Nat. Rev. Drug Discov. 20 (2021) 899–919, https://doi.org/10.1038/s41573-021-00155-y.
[5] N. Patsoukis, Q. Wang, L. Strauss, V.A. Boussiotis, Revisiting the PD-1 pathway, Sci. Adv. 38 (6) (2020) eabd2712. https://doi:10.1126/sciadv.
[6] Z. Liu, H. Zhang, J. Sun, M. Zhang, L. Cui, Y. Zhang, J. Cheng, Z. Tang, Organic-solvent-free "lego-like" modular preparation of fab-nondestructive antibody-drug conjugates with ultra-high drug-to-antibody ratio, Adv. Mater. 8 (2023) e2300377, https://doi.org/10.1002/adma.202300377.
[7] T. Shan, S. Chen, T. Wu, Y. Yang, S. Li, X. Chen, Pd-l1 expression in colon cancer and its relationship with clinical prognosis, Int. J. Clin. Exp. Pathol. 12 (5) (2019) 1764–1769. https://pubmed.ncbi.nlm.nih.gov/31933995.
[8] W. Yu, Y. Hua, H. Qiu, J. Hao, K. Zou, Z. Li, S. Hu, P. Guo, M. Chen, S. Sui, Y. Xiong, F. Li, J. Lu, W. Guo, G. Luo, W. Deng, PD-L1 promotes tumor growth and progression by activating wip and β-catenin signaling pathways and predicts poor prognosis in lung cancer, Cell Death Dis. 11 (2020) 506, https://doi.org/10.1038/s41419-020-2701-z.
[9] Q. Wu, L. Jiang, S. Li, Q. He, B. Yang, J. Cao, Small molecule inhibitors targeting the PD-1/PD-L1 signaling pathway, Acta Pharmacol. Sin. 42 (1) (2021) 1–9, https://doi.org/10.1038/s41401-020-0366-x.
[10] S. Kleffel, C. Posch, S.R. Barthel, H. Mueller, C. Schlapbach, E. Guenova, C.P. Elco, N. Lee, V. Juneja, Q. Zhan, C.G. Lian, R. Thomi, W. Hoetzenecker, A. Cozzio, R. Dummer, M.C. Mihm Jr., K.T. Flaherty, M.H. Frank, G.F. Murphy, A.H. Sharpe,

T.S. Kupper, T. Schatton, Melanoma cell-intrinsic PD-1 receptor functions promote tumor growth, Cell 162 (6) (2015) 1242–1256. https://doi:10.1016/j.cell.2015.08.052.
[11] L. Gandhi, D. Rodríguez-Abreu, S. Gadgeel, Pembrolizumab plus chemotherapy in metastatic non-small-cell lung cancer, N. Engl. J. Med. 378 (2018) 2078–2092. https://doi:10.1056/NEJMoa1801005.
[12] J.R. Brahmer, C.G. Drake, I. Wollner, J.D. Powderly, J. Picus, W.H. Sharfman, E. Stankevich, A. Pons, T.M. Salay, Phase i study of single-agent anti-programmed death-1 (mdx-1106) in refractory solid tumors: safety, clinical activity, pharmacodynamics, and immunologic correlates, J. Clin. Oncol. 28 (19) (2010) 3167–3175. https://doi:10.1200/JCO.2009.26.7609.
[13] S.L. Topalian, F.S. Hodi, J.R. Brahmer, S.N. Gettinger, D.C. Smith, D.F. McDermott, J.D. Powderly, R.D. Carvajal, J.A. Sosman, M.B. Atkins, P.D. Leming, D.R. Spigel, S. J. Antonia, L. Horn, C.G. Drake, D.M. Pardoll, L. Chen, W.H. Sharfman, R. A. Anders, J.M. Taube, T.L. McMiller, H. Xu, A.J. Korman, M.J. Kunkel, S. Agrawal, D. McDonald, G.D. Kollia, A. Gupta, J.M. Wigginton, M. Sznol, Safety, activity, and immune correlates of anti-pd-1 antibody in cancer, N. Engl. J. Med. 366 (26) (2012) 2443–2454. https://doi:10.1056/NEJMoa1200690.
[14] J. Sun, Z. Liu, H. Yao, H. Zhang, M. Zheng, N. Shen, J. Cheng, Z. Tang, X. Chen, Azide-masked resiquimod activated by hypoxia for selective tumor therapy, Adv Mater 35 (29) (2023) e2207733. https://doi:10.1002/adma.202207733.
[15] R.S. Herbst, P. Baas, D.W. Kim, E. Felip, J.P. Gracia, J. Han, J. Molina, J. Kim, C. D. Arvis, M. Ahn, M. Majem, M.J. Fidler, G. Castro, M. Garrido, G.M. Lubiniecki, Y. Shentu, E. Im, M. Filhart, E. Garon, Pembrolizumab versus docetaxel for previously treated, pd-l1-positive, advanced non-small-cell lung cancer (keynote-010): a randomised controlled trial, Lancet 387 (2016) 1540–1550. https://doi:10.1016/S0140-6736(15)01281-7.
[16] M. Reck, R. Abreu, A. Robinson, R. Hui, T. Csoszi, A. Fulop, M. Gottfried, N. Peled, A. Tafreshi, S. Cuffe, M. Brien, S. Rao, K. Hotta, M.A. Leiby, G.M. Lubiniecki, Y. Shentu, R. Rangwala, J.R. Brahmer, A.G. Robinson Ag, Pembrolizumab versus chemotherapy for pd-l1-positive non-small-cell lung cancer, N. Engl. J. Med. 375 (19) (2016) 1823–1833. https://doi:10.1056/NEJMoa1606774.
[17] J. Brahmer, K.L. Reckamp, P. Baas, L. Crino, W.E. Eberhardt, E. Poddubskaya, S. Antonia, A. Pluzanski, W.E. Eberhardt, E. Poddubskaya, S. Antonia, A. Pluzanski, E. Vokes, E. Holgado, D. Waterhouse, N. Ready, J. Gainor, O. Frontera, L. Havel, M. Steins, M.C. Garassino, J.G. Aerts, M. Domine, L. Ares, M. Reck, C. Baudelet, C. Harbison, B. Lestini, D.R. Spigel, Nivolumab versus docetaxel in advanced squamous-cell non-small-cell lung cancer, N. Engl. J. Med. 373 (2) (2015) 123–135. https://doi:10.1056/NEJMoa1504627.
[18] M.E. Goebeler, R.C. Bargou, T cell-engaging therapies — bites and beyond, Nat. Rev. Clin. Oncol. 17 (7) (2020) 418–434. https://doi:10.1038/s41571-020-0347-5.
[19] X. Yang, X. Lin, W. Shi, S. Xie, X. Huang, S. Yin, X. Jiang, Nanobody-based bispecific t-cell engager (nb-bite): a new platform for enhanced t-cell immunotherapy, Sig Transduct Target Ther 328 (8) (2023), https://doi.org/10.1038/s41392-023-01523-3.
[20] M.E. Goebeler, R. Bargou, Blinatumomab: a cd19/cd3 bispecific t cell engager (bite) with unique anti-tumor efficacy, Leuk. Lymphoma 57 (5) (2016) 1021–1032. https://doi:10.3109/10428194.2016.1161185.
[21] M.R. Middleton, C. McAlpine, V.K. Woodcock, P. Corrie, J. Infante, N.M. Steven, T. R. Evans, A. Anthoney, Tebentafusp, a tcr/anti-cd3 bispecific fusion protein targeting gp100, potently activated antitumor immune responses in patients with metastatic melanoma, Clin. Cancer Res. 26 (22) (2020) 5869–5878. https://doi:10.1158/1078-0432.CCR-20-1247.
[22] L.E. Budde, L.H. Sehn, M. Matasar, S.J. Schuster, S. Assouline, P. Giri, J. Kuruvilla, M. Canales, S. Dietrich, K. Fay, M. Ku, L. Nastoupil, C.Y. Cheah, M.C. Wei, S. Yin, C. Li, H. Huang, A. Kwan, E. Penuel, N.L. Bartlett, Safety and efficacy of mosunetuzumab, a bispecific antibody, in patients with relapsed or refractory follicular lymphoma: a single-arm, multicentre, phase 2 study, Lancet Oncol. 23 (8) (2022) 1055–1065. https://doi:10.1016/S1470-2045(22)00335-7.
[23] S.Z. Usmani, A.L. Garfall, N. Donk, H. Nahi, J. Miguel, A. Oriol, L. Rosinol, A. Chari, M. Bhutani, L. Karlin, L. Benboubker, L. Pei, R. Verona, S. Girgis, T. Stephenson, Y. Elsayed, J. Infante, J.D. Goldberg, A. Banerjee, M. Mateos, A. Krishnan, Teclistamab, a b-cell maturation antigen × CD3 bispecific antibody, in patients with relapsed or refractory multiple myeloma (majestec-1): a multicentre, open-label, single-arm, phase 1 study, Lancet 398 (2021) 665–674. https://doi:10.1016/S0140-6736(21)01338-6.
[24] M. Noguchi-Sasaki, T. Soeda, A. Ueyama, A. Muto, M. Hirata, H. Kitamura, K. Ouchi, Y. Kawabe, K. Nogami, M. Shima, T. Kitazawa, Emicizumab, a bispecific antibody to factors ix/ixa and x/xa, does not interfere with antithrombin or tfpi activity in vitro, TH Open 2 (1) (2018) e96–e103. https://doi:10.1055/s-0038-1636538.
[25] A.I. Segaliny, J. Jayaraman, X. Chen, J. Chong, R. Luxon, A. Fung, Q. Fu, X. Jiang, R. Rivera, X. Ma, C. Ren, J. Zimak, P.N. Hedde, Y. Shang, G. Wu, W. Zhao, A high throughput bispecific antibody discovery pipeline, Commun. Biol. 380 (6) (2023), https://doi.org/10.1038/s42003-023-04746-w.
[26] A.F. Labrijn, M.L. Janmaat, J.M. Reichert, P. Parren, Bispecific antibodies: a mechanistic review of the pipeline, Nat. Rev. Drug Discov. 18 (8) (2019) 585–608. https://doi:10.1038/s41573-019-0028-1.
[27] Y. Gong, L. Zhang, J. Li, S. Feng, H. Deng, Development of the double cyclic peptide ligand for antibody purification and protein detection, Bioconjug Chem 27 (7) (2016) 1569–1573. https://doi:10.1021/acs.bioconjchem.6b00170.
[28] F. Xue, H. Yao, L. Cui, Y. Huang, C. Shao, N. Shen, J. Hu, Z. Tang, X. Chen, An fc binding peptide-based facile and versatile build platform for multispecific antibodies, Nano Lett. 23 (10) (2023) 4191–4200. https://doi:10.1021/acs.nanolett.3c00071.
[29] Y. Gong, M. Yi, L. Zhang, S. Feng, H. Deng, Characterization of the Fc-III-4C-based recombinant protein expression system by using carbonic anhydrase as the model protein, Protein Expr. Purif. 177 (2021) 105761. https://doi:10.1016/j.pep.2020.105761.
[30] K. Sasaki, M. Harada, Y. Miyashita, H. Tagawa, A. Kishimura, T. Mori, Y. Katayama, Fc-binding antibody-recruiting molecules exploit endogenous antibodies for anti-tumor immune responses, Chem. Sci. 11 (2020) 3208–3214, https://doi.org/10.1039/D0SC00017E.
[31] H. Yu, Z. Tang, D. Zhang, W. Song, Y. Zhang, Y. Yang, Z. Ahmad, X. Chen, Cisplatin loaded poly(l-glutamic acid)-g-methoxy poly(ethylene glycol) complex nanoparticles for potential cancer therapy: preparation, in vitro and in vivo evaluation, J. Biomed. Nanotechnol. 12 (2016) 69–78, https://doi.org/10.1166/jbn.2016.2152.
[32] L. Zhao, C. Xiao, L. Wang, G. Gai, J. Ding, Glucose-sensitive polymer nanoparticles for self-regulated drug delivery, Chem. Commun. 52 (49) (2016) 7633–7652. https://doi:10.1039/c6cc02202b.
[33] C. Li, Poly(l-glutamic acid)–anticancer drug conjugates, Adv. Drug Deliv. Rev. 54 (5) (2002) 695–713. https://doi:10.1016/s0169-409x(02)00045-5.
[34] P. Darvin, S.M. Toor, V. Sasidharan, E. Elkord, Immune checkpoint inhibitors: recent progress and potential biomarkers, Exp. Mol. Med. 50 (12) (2018) 1–11. https://doi:10.1038/s12276-018-0191-1.
[35] P. Darvin, S.M. Toor, V. Sasidharan, E. Elkord, Erratum: molecular mechanisms of t cell co-stimulation and co-inhibition, Nat. Rev. Immunol. 13 (4) (2013), 542-542, https://doi:10.1038/nri3405.
[36] I. Mellman, G. Coukos, G. Dranoff, Cancer immunotherapy comes of age, Nature 480 (7378) (2011) 480–489. https://doi:10.1038/nature10673.
[37] J.Y. Zhang, Y.Y. Yan, J. Li, R. Adhikari, L. Fu, PD-1/PD-L1 based combinational cancer therapy: icing on the cake, Front. Pharmacol. 11 (2020) 722. https://doi:10.3389/fphar.2020.00722.
[38] D.M. Pardoll, The blockade of immune checkpoints in cancer immunotherapy, Nat. Rev. Cancer 12 (4) (2012) 252–264. https://doi:10.1038/nrc3239.
[39] H. Yao, N. Shen, G. Ji, J. Huang, J. Sun, G. Wang, Z. Tang, X. Chen, Cisplatin nanoparticles promote intratumoral CD8($^{+}$) T cell priming via antigen presentation and t cell receptor crosstalk, Nano Lett. 22 (8) (2022) 3328–3339. https://doi:10.1021/acs.nanolett.2c00478.
[40] R. Yang, S. Shen, C. Gong, X. Wang, F. Luo, F. Luo, Y. Lei, Z. Wang, S. Xu, Q. Ni, Y. Xue, Z. Fu, L. Zeng, L. Fang, Y. Yan, J. Zhang, L. Gan, J. Yi, P. Zhou, Bispecific antibody PL-L1 x CD3 boosts the anti-tumor potency of the expanded vgamma2vdelta2 t cells, Front. Immunol. 12 (2021) 654080. https://doi:10.3389/fimmu.2021.654080.
[41] L. Gattinoni, N.P. Restifo, Moving t memory stem cells to the clinic, Blood 121 (4) (2013) 567–568. https://doi:10.1182/blood-2012-11-468660.
[42] M. Takeshita, K. Suzuki, Y. Kassai, M. Takiguchi, Y. Nakayama, Y. Otomo, R. Morita, T. Miyazaki, A. Yoshimura, T. Takeuchi, Polarization diversity of human CD4^{+} stem cell memory t cells, Clinical Immunol. 159 (1) (2015) 107–117. https://doi:10.1016/j.clim.2015.04.010.
[43] R. Parihar, J. Dierksheide, Y. Hu, W.E. Carson, Il-12 enhances the natural killer cell cytokine response to ab-coated tumor cells, J. Clin. Invest. 110 (7) (2002) 983–992. https://doi:10.1172/JCI15950.
[44] C. Becker, S. Wirtz, M.F. Neurath, M.F. Neurath, Stepwise regulation of th1 responses in autoimmunity: il-12-related cytokines and their receptors, Inflamm. Bowel Dis. 11 (8) (2005) 755–764. https://doi:10.1097/01.mib.0000172808.03877.4d.
[45] D.I. Jang, A.H. Lee, H.Y. Shin, H.R. Song, J.H. Park, T.B. Kang, S.R. Lee, S.H. Yang, The role of tumor necrosis factor alpha (TNF-α) in autoimmune disease and current tnf-α inhibitors in therapeutics, Int. J. Mol. Sci. 22 (5) (2021) 2719. https://doi:10.3390/ijms22052719.
[46] S. Wang, G. Yu, W. Yang, Z. Wang, O. Jacobson, H. Deng, L. Lin, X. Chen, Photodynamic-chemodynamic cascade reactions for efficient drug delivery and enhanced combination therapy, Adv. Sci. 8 (10) (2021) 2002927. https://doi:10.1002/advs.202002927.